Supporting Information

Ultra-high resolution, multi-scenario, super-elastic inductive strain sensors based on liquid metal for the wireless monitoring of human movement

Jian Mao[a,b,c], Zidong He[b,c]*, Yuanzhao Wu[b,c], Jinwei Cao[f], Shijing Zhao[b,c], Bin Chen[a,b,c], Jie Shang[b,c], Yiwei Liu[b,c,d]*, Run-Wei Li[b,c,d,e]*

a) Faculty of Electrical Engineering and Computer Science, Ningbo University, Ningbo, Zhejiang 315211, China

b) CAS Key Laboratory of Magnetic Materials and Devices, Ningbo Institute of Materials Technology and Engineering, Chinese Academy of Sciences, Ningbo, Zhejiang 315201, China

c) Zhejiang Province Key Laboratory of Magnetic Materials and Application Technology, Ningbo Institute of Materials Technology and Engineering, Chinese Academy of Sciences, Ningbo, Zhejiang 315201, China

d) Center of Materials Science and Optoelectronics Engineering, University of Chinese Academy of Sciences, Beijing 100049, China

e) School of Future Technology, University of Chinese Academy of Sciences, Beijing 100049, China

f) Innovative Center for Flexible Devices (iFLEX), Max Planck-NTU Joint Lab for Artificial Senses, School of Materials Science and Engineering, Nanyang Technological University, 50 Nanyang Avenue, 639798, Singapore.

*Corresponding author
E-mail: runweili@nimte.ac.cn (Prof. Run-Wei Li); liuyw@nimte.ac.cn (Prof. Yiwei Liu); hezidong@nimte.ac.cn (Dr. Zidong He).

This file contains:

Supplementary Texts 1-2

Figures S1 to S5

Captions for Movies S1 to S3

References

Other Supplementary Materials for this manuscript include the following:

Video S1：
Performance of the system in terms of detecting different breathing patterns of the mannequin.

Video S2：
The capabilities of detection of respiration by the sensor when affixed to the human chest during running, walking, and at rest.

Video S3：
The developed human motion monitoring system detects both respiratory signals and joint movements during human motion.

Supplementary Text 1

The diagram below illustrates the transformation of the coil's shape within the sensor as it undergoes stretching. The width of the conductor perpendicular to the direction of stretching decreases as the length increases. Conversely, the length of the conductor parallel to the stretching direction decreases while the width increases. In figure a, L represents the side length of the square coil, s is the distance between two parallel wire segments, w is the width of the wires, and d is the spatial distance between the wires.

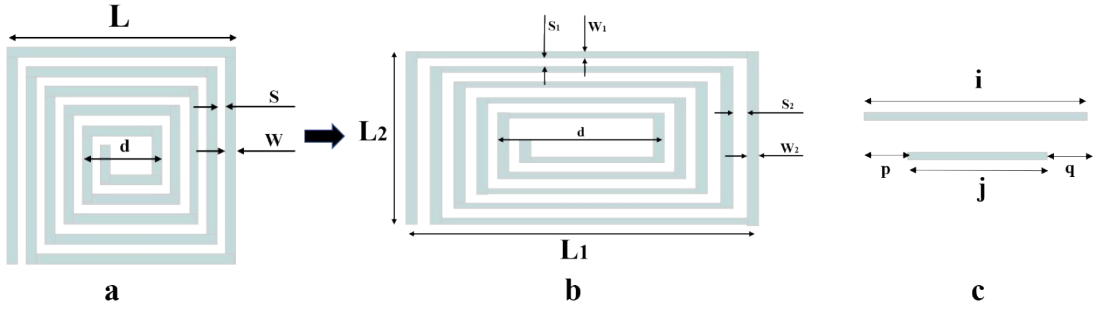

Supplementary Text 2

Moving average filtering

$$y(n) = \frac{1}{2m+1}\sum_{n-m}^{n+m}(n-k) \tag{1}$$

The moving average filter treats N consecutive sampled values as a queue with a fixed length of N. Each time a new data point is sampled, it is added to the end of the queue, and the oldest data point at the front of the queue is discarded. The average of the N data points in the queue is then calculated to obtain the new filtered result. After applying the moving average filter, the overall waveform becomes smoother. Here, m is a positive integer, L=2m+1 is the filter order, which is also equal to the width of the moving window. Through practical testing, we have selected a window width of 16, ensuring both filtering effectiveness and real-time data processing.

Supplementary Figures

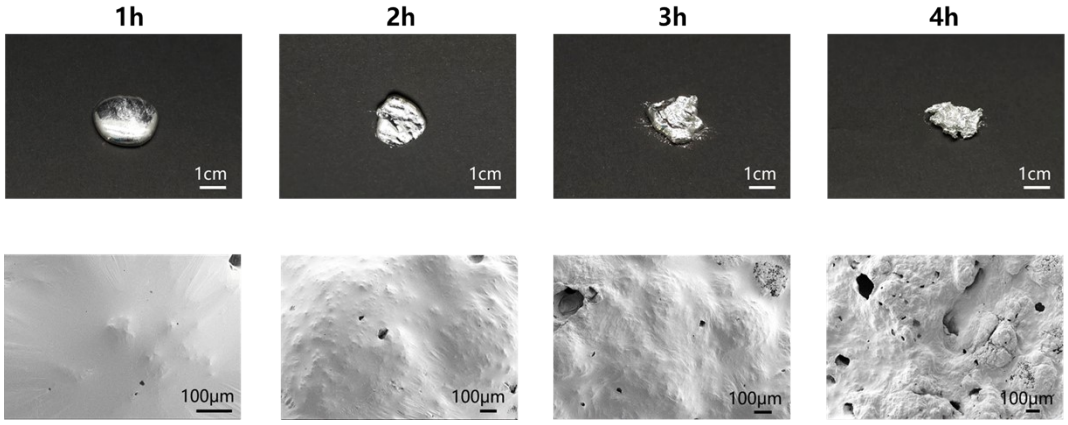

Fig. S1 Optical and SEM images of liquid metal after 1-4h oxidation.

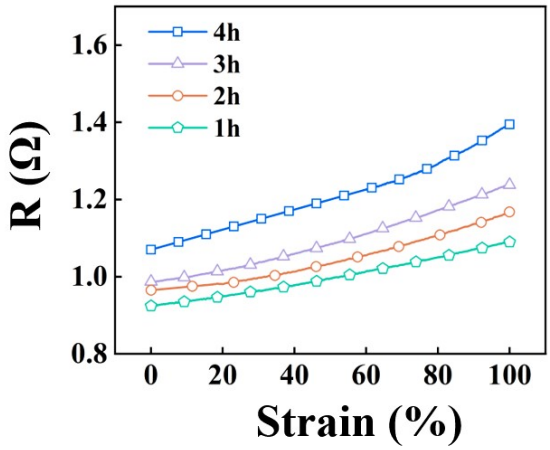

Fig. S2. Resistance changes in liquid metal after 1-4 hours of oxidation when subjected to 0-100% stretching.

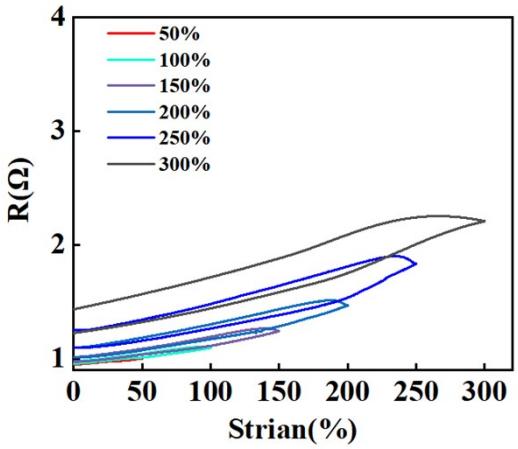

Fig. S3. The change of resistance in strain of liquid metal putty at different tensile strains (0 to 300% of strain, Sample's length and width: 30*5 mm).

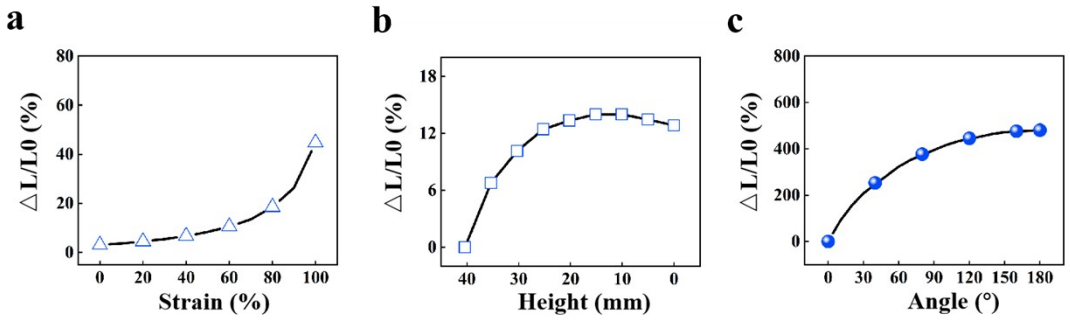

Fig. S4. Finite Element Method Simulation of Sensors under Tension, Bending, and Folding Conditions. (a) Relative inductance variation as the sensor is stretched from 0% to 100% strain. (b) Relative change in inductance for different bending deformations. (c) Relative inductance variation at different folding angles.

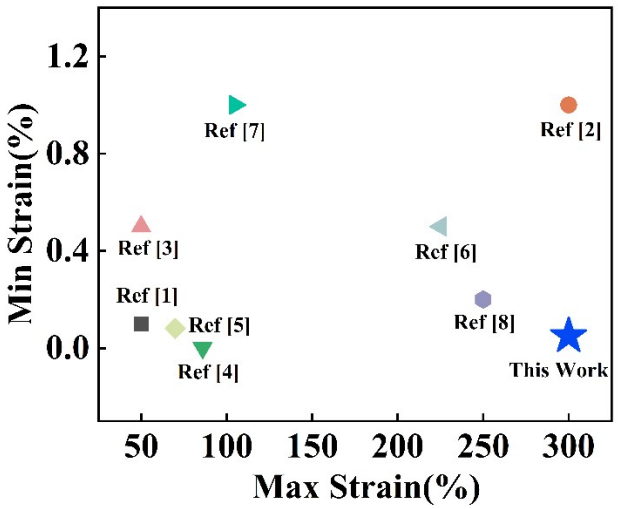

Fig. S5. Comparison of maximum stretchability and minimum strain detection with other flexible wearable strain sensors.[1-8]

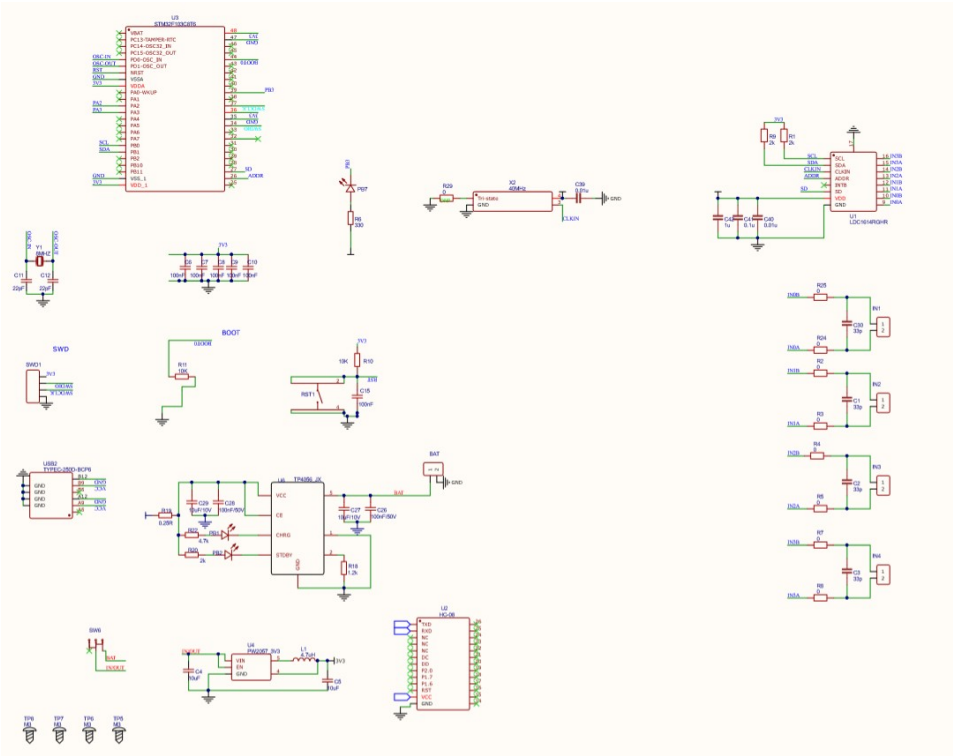

Fig. S6. The schematic of the sensor signal acquisition circuit.

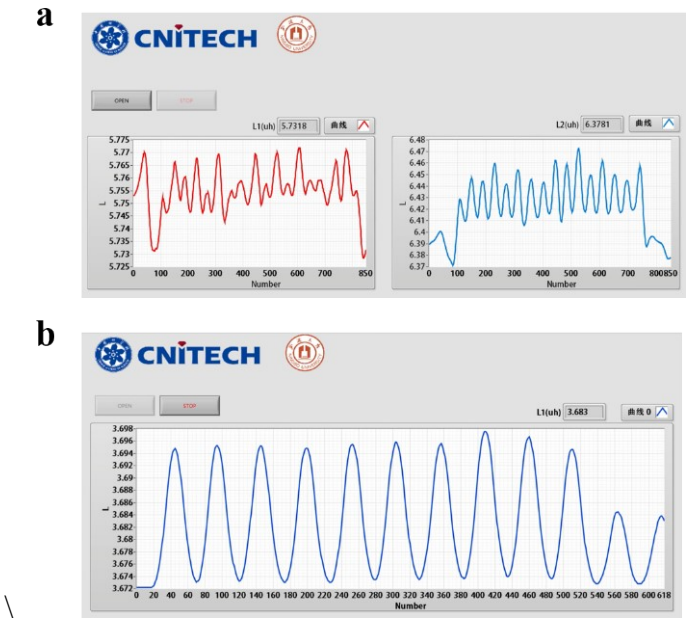

Fig. S7. Displaying the data collected by the sensor on LabVIEW. (a) Dual-channel display interface. (b) Single-channel display interface.

References

1. S. Wang, X. Yi, Y. Zhang, Z. Gao, Z. Xiang, Y. Wang, Y. Wu, Y. Liu, J. Shang and R.-W. Li, *Chemosensors*, 2023, **11**, 270.
2. L. Cai, L. Song, P. Luan, Q. Zhang, N. Zhang, Q. Gao, D. Zhao, X. Zhang, M. Tu and F. Yang, *Scientific reports*, 2013, **3**, 3048.
3. M. Amjadi, M. Turan, C. P. Clementson and M. Sitti, *ACS applied materials & interfaces*, 2016, **8**, 5618-5626.
4. J. Ramírez, D. Rodriquez, A. D. Urbina, A. M. Cardenas and D. J. Lipomi, *ACS applied nano materials*, 2019, **2**, 2222-2229.
5. Y. R. Jeong, H. Park, S. W. Jin, S. Y. Hong, S. S. Lee and J. S. Ha, *Advanced Functional Materials*, 2015, **25**, 4228-4236.
6. Y. Zhao, M. Ren, Y. Shang, J. Li, S. Wang, W. Zhai, G. Zheng, K. Dai, C. Liu and C. Shen, *Composites Science and Technology*, 2020, **200**, 108448.
7. J. Pan, M. Yang, L. Luo, A. Xu, B. Tang, D. Cheng, G. Cai and X. Wang, *ACS applied materials & interfaces*, 2019, **11**, 7338-7348.
8. O. Atalay, A. Atalay, J. Gafford, H. Wang, R. Wood and C. Walsh, *Advanced Materials Technologies*, 2017, **2**, 1700081.